electronics

MDPI

Article

Simulation of High-Voltage Cable Sheath Current with a Panoramic Digital Tunnel Model

Zehua Pan [1], Wei Guo [1], Yekun Men [1], Jing Cai [1], Huachun Li [1], Long Xiao [2], Shiru Xu [2], Yu Wang [2] and Yuanxi Li [2,*]

[1] State Grid Beijing Electric Power Research Institute, Beijing 100075, China; panzehua@bj.sgcc.com.cn (Z.P.); guowei@bj.sgcc.com.cn (W.G.); menyekun@bj.sgcc.com.cn (Y.M.); caijing@bj.sgcc.com.cn (J.C.); lihuachun@bj.sgcc.com.cn (H.L.)

[2] School of Electrical Engineering and Automation, Wuhan University, Wuhan 430072, China; 622210900001@mails.cqjtu.edu.cn (L.X.); xushiru@whu.edu.cn (S.X.); yuwang@whu.edu.cn (Y.W.)

* Correspondence: liyuanxi@whu.edu.cn

Abstract: Monitoring cable sheath current is crucial for guaranteeing the secure and efficient operation of high-voltage cable tunnels. In this study, a three-dimensional (3D) panoramic digital model of a tunnel in Beijing is modeled, a parallel cable sheath current simulation model is proposed, and a 3D panoramic visualization system with which the cable sheath current can be simulated online is developed in order to generate early warnings on the sheath current situation. The accuracy of the simulation model is verified and the results are as follows: The difference between the simulated sheath current and the actual measurement is within a maximum margin of 3.71%. A phase sequence optimization strategy can be obtained after calculations based on the simulation model, and an average sheath current reduction of 47.2% can be achieved following the optimization strategy. This study introduces a new approach by which cable sheath current dynamics and real-time warning against anomalies are visualized on a 3D tunnel model. In addition, a sheath current simulation model is integrated in the 3D visualization system developed in this study, and phase sequence optimization strategies for cables with abnormal sheath currents are automatically suggested, which may provide scientific support for auxiliary decision-making in real-time cable operation.

Keywords: high-voltage cable tunnel; three-dimensional digital model; sheath current simulation; phase sequence optimization

check for updates

Citation: Pan, Z.; Guo, W.; Men, Y.; Cai, J.; Li, H.; Xiao, L.; Xu, S.; Wang, Y.; Li, Y. Simulation of High-Voltage Cable Sheath Current with a Panoramic Digital Tunnel Model. *Electronics* **2024**, *13*, 4884. https://doi.org/10.3390/electronics13244884

Academic Editor: Spyridon Nikolaidis

Received: 12 November 2024
Revised: 5 December 2024
Accepted: 9 December 2024
Published: 11 December 2024

Copyright: © 2024 by the authors. Licensee MDPI, Basel, Switzerland. This article is an open access article distributed under the terms and conditions of the Creative Commons Attribution (CC BY) license (https://creativecommons.org/licenses/by/4.0/).

1. Introduction

Currently, the monitoring of cable sheath currents at all joints of high-voltage cable lines in the Beijing area has been preliminarily implemented [1–3]. However, due to limitations in the installation environment and sensor data transmission, issues such as data loss, temporal misalignment, update delays, and inefficient information exchange often arise during practical application, reflecting deficiencies in the digitalization and intelligent development of the power grid [4]. If abnormal sheath currents occur in locations with missing data, the system will be unable to detect the anomaly and provide an early warning. Excessive sheath currents can lead to increased thermal losses in the cable, reducing its current-carrying capacity. In severe cases, this may cause cable joints and grounding boxes to burn out, severely affecting the safe and stable operation of the cable and increasing unnecessary inspection costs [5–7].

Digital twins, a representative technology for digital and intelligent operation and maintenance, have successfully been applied in the power industry [8–12]. Guo et al. [13] use approaches like the Cahn–Hilliard equation to effectively model and rectify the damaged regions of digital representations. In the field of cable tunnel digital twins, several studies have utilized laser scanning technology to construct 3D models of cable tunnels [14–16]. Temperature is regarded as a key parameter in the modelling of monitoring models for high-voltage cables [17–22]. Zhou et al. [23] and Zhu et al. [24] developed digital models

for substation cables, enabling the visualization of cable systems within substations. In the field of the analysis and calculation of cable sheath circulating currents, some studies have focused on the determinants of cable sheath currents and analyzed the impacts of different factors on sheath currents [25–30]. Some [31–35] have studied the impact of the uneven cross-interconnection segmentation of multi-circuit cables on cable sheath currents, while others [36–38] have analyzed the causes of zero-sequence current in cables, considering a dual-circuit cable system as a case study. In the field of sheath current standards, both the State Grid Corporation of China and China Southern Power Grid have formulated corresponding enterprise standards, which propose operational and maintenance regulations for high-voltage cables based on sheath current limits [39,40]. In conclusion, current applications of digital twin technology are primarily focused on scene and substation modeling, and are mainly used to monitor the surface temperature of cables. However, research on monitoring and applying key parameters of the cable remains to be studied.

In this study, a 3D panoramic digital model of a tunnel in Beijing is modeled, a parallel cable sheath current simulation model is proposed, and a panoramic visualization system is developed that is capable of online sheath current simulation and giving early warnings related to sheath current conditions. By comparing the computed sheath current with sensor measurements, the results demonstrate the reliability of the proposed simulation model. Using this visualization system, the sheath current within monitoring gaps is inferred, enabling the visualization of sheath current across entire cable lines. Based on the sheath current simulation of cables in this tunnel, phase sequence optimization strategies for cables exhibiting abnormal sheath currents are automatically suggested, which provides scientific decision support for sheath current suppression and regulation.

2. Three-Dimensional Panoramic Digital Modeling of the Tunnel

2.1. Technological Route

The overall technical route for the 3D panoramic digital modeling of the cable tunnel is presented in Figure 1, consisting of three key steps: (1) 3D Data Acquisition: Terrestrial laser scanning (TLS) technology is employed to collect complete point cloud data of the transmission tunnel by placing targets and setting up multiple scanning stations in the tunnel. (2) Point Cloud Pre-processing: The point cloud data from each station are pre-processed through alignment, stitching, denoising, and other techniques. (3) Tunnel Digital Modeling: The initial 3D model is established based on the processed point cloud data using modeling software. Subsequently, photographs of the tunnels, cables, and ancillary equipment are taken with a digital camera, followed by texture creation and mapping onto the model.

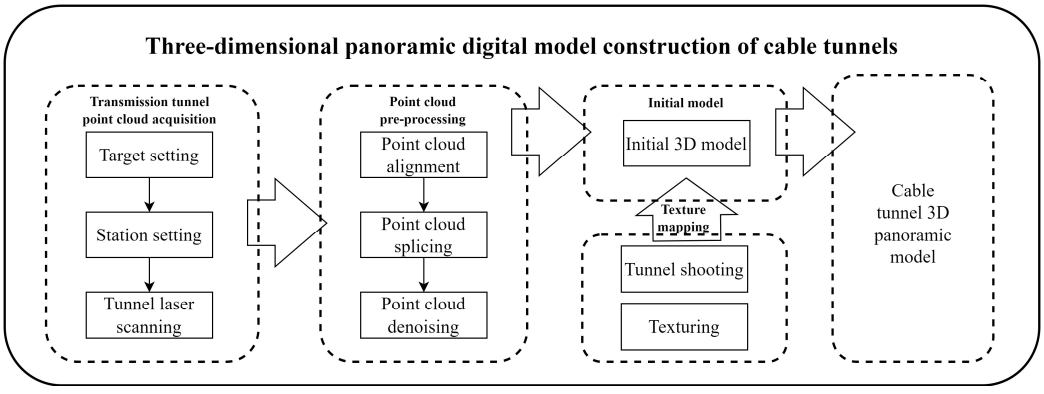


Figure 1. Flowchart of digital twin modeling technology for cable tunnel.

2.2. Spatial Data Acquisition

In this study, a FARO S350 3D laser scanner is utilized to acquire the point cloud data of the tunnel. Since cable tunnels usually extend from hundreds to thousands of meters,

and given the limitations of the scanner's accuracy, as well as the tunnel's layout, multiple scanning stations are required. To ensure the proper alignment and splicing of the point cloud, overlapping scanning areas are necessary between adjacent stations, and targets are placed within a specified range in front of and behind each scanner, respectively. Once the scanning process is completed, a panoramic depth image is generated, as shown in Figure 2.

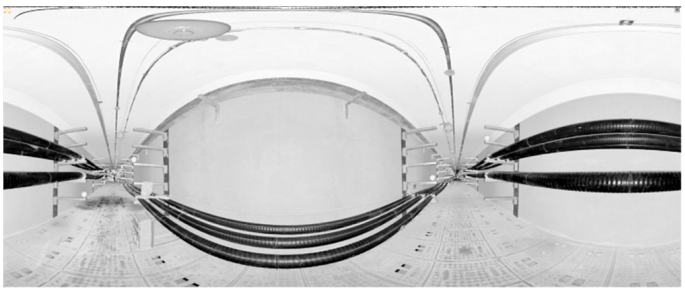


Figure 2. Scanning panoramic depth image map.

2.3. Point Cloud Data Processing

To establish the complete point cloud data of the cable tunnel, it is necessary to align the point clouds collected from multiple stations into the same coordinate reference system. Point cloud alignment usually consists of two stages: coarse alignment and fine alignment. Coarse alignment is achieved by selecting a minimum of four corresponding feature points between two adjacent scanning stations, calculating the translation and rotation matrices, and then performing a coordinate transformation. Fine alignment further reduces alignment errors by refining the initial point cloud through leveling the roughly spliced point cloud based on the target sphere and the control points arranged during station setup. Once each station is aligned, the point clouds can be integrated to form the comprehensive point cloud data of the tunnel. In addition, the point cloud data of the cable tunnel obtained by the terrestrial laser scanning instrument may contain noise or irrelevant data, which must be removed before 3D modeling.

2.4. Three-Dimensional Modeling and Texture Mapping

An SLR digital camera is used to photograph the floor, walls, equipment, sign nameplates, etc., within the cable tunnel in order to obtain the corresponding texture information. Then, Photoshop software (Version 23.1) is used to process the collected photos, thereby obtaining the texture information of the object surfaces within the tunnel.

The 3D digital model of the tunnel is established with 3Ds MAX modeling software (Version 2023.1). Subsequently, the texture data are mapped onto the relevant model.

Eventually, a 3D panoramic digital model of the cable tunnel is modeled, as shown in Figure 3.

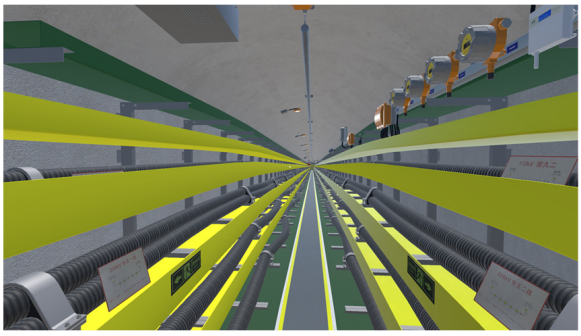


Figure 3. Exhibition of the modeled tunnel.

3. High-Voltage Cable Sheath Current Simulation Model Set up and Validation

3.1. Parallel Cable Sheath Current Simulation Model

When the cable line is long (more than 1000 m), the cable metal sheath is generally grounded through a cross-interconnection protector. The cable is divided into three multiples of equal length, establishing small segments, and each small segment is connected with an insulated connector. The metal sheathing of each segment is routed via a coaxial cable to a cross-interconnection box for relocation, and the termination of each cross-interconnection section is directly grounded. The cross-interconnection grounding method is shown in Figure 4.

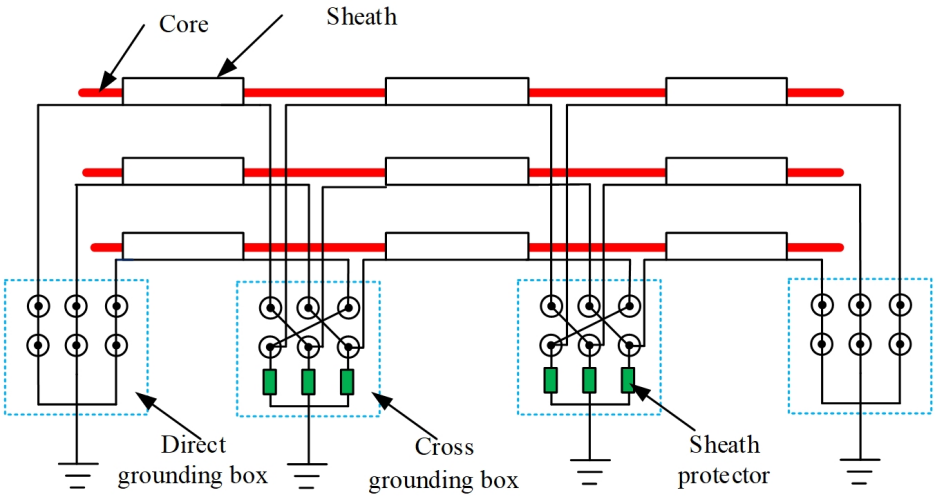


Figure 4. Schematic diagram of cross-interconnection grounding method.

Due to the existence of electromagnetic induction between metal conductors, when there is a current flowing in the cable core, a current will be induced in the metal sheath, and the induced electromotive force on the sheath will be generated by the core current together with the sheath current. According to the definition of the cross-interconnection grounding method, the equivalent circuit diagram of the cable cross-interconnection system is shown in Figure 5. Z_1, Z_2, , Z_3 are the impedance of each small segment of the sheath, respectively, $\dot{E}_{ti,j}$ is the induced electromotive force generated by the sheath current, and $\dot{E}_{si,j}$ is the induced electromotive force generated by the core current. $\dot{I}_{s1}$, $\dot{I}_{s2}$, $\dot{I}_{s3}$ are the sheath current of each single cable, respectively, and R_{d1}, R_{d2} are the grounding resistance.

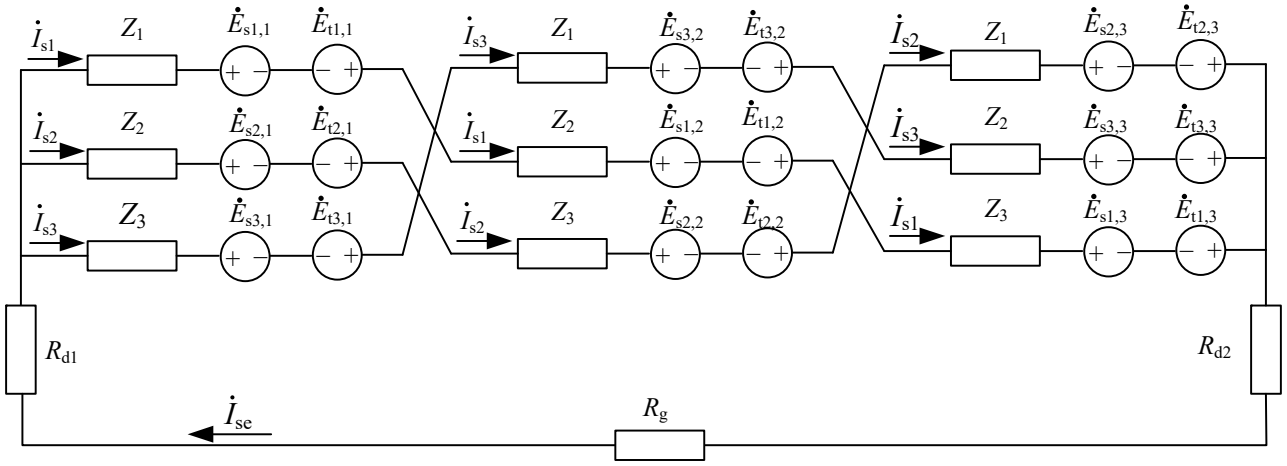


Figure 5. Equivalent circuit diagram for cross-interconnection of single-circuit cable.

For a single-circuit cable, the self-inductive and mutual inductive resistance per unit length of the i_{th} cable's metal sheath can be calculated as follows:

$$X_{\mathrm{i}} = 4\pi f \times 10^{-7} \ln\left(\frac{D_{\mathrm{e}}}{r_{i,\mathrm{GMR}}}\right)(\Omega/\mathrm{m}) \tag{1}$$

$$X_{ij} = 4\pi f \times 10^{-7} \ln\left(\frac{D_{\mathrm{e}}}{s_{ij}}\right)(\Omega/\mathrm{m}) \tag{2}$$

$$D_e = 660\sqrt{\left(\frac{\rho_g}{h}\right)} \tag{3}$$

$$r_{i_{GMR}} = \frac{(d_{s1i} + d_{s2i})}{2} \times 10^{-3} \tag{4}$$

where X_i is the self-induced resistance per unit length of the i_{th} metal sheath, D_e is the earth-equivalent circuit depth (unit: m), s_{ij} is the center distance between conductor i and conductor j (unit: m), ρ_g is the earth resistivity (unit Ω), f is the core current frequency (unit: Hz), $r_{i_{GMR}}$ is the geometric mean radius of the metal sheath of the i_{th} metal sheath cable, d_{s1i} is the i_{th} metal sheath inner diameter (unit: mm), and d_{s2i} is the i_{th} metal sheath outer diameter (unit: mm).

Taking a single-circuit cable as an example, let the numbers of phase A, phase B, and phase C be 1, 2, and 3, respectively. The total induced voltage generated on the sheath of a phase of the circuit contains the induced voltage generated by the core currents of three phases and the induced voltage generated by the sheath currents of the other two phases.

The induced voltage generated by the core currents on the sheath can be calculated as follows:

$$\begin{bmatrix} \dot{E}_{\mathrm{t1}} \\ \dot{E}_{\mathrm{t2}} \\ \dot{E}_{\mathrm{t3}} \end{bmatrix} = -\mathrm{j}\begin{bmatrix} X_{11}l_1 + X_{21}l_2 + X_{31}l_3 & X_{12}l_1 + X_{22}l_2 + X_{32}l_3 & X_{13}l_1 + X_{23}l_2 + X_{33}l_3 \\ X_{21}l_1 + X_{31}l_2 + X_{11}l_3 & X_{22}l_1 + X_{32}l_2 + X_{12}l_3 & X_{23}l_1 + X_{33}l_2 + X_{13}l_3 \\ X_{31}l_1 + X_{11}l_2 + X_{21}l_3 & X_{32}l_1 + X_{12}l_2 + X_{22}l_3 & X_{33}l_1 + X_{13}l_2 + X_{23}l_3 \end{bmatrix}\begin{bmatrix} \dot{I}_1 \\ \dot{I}_2 \\ \dot{I}_3 \end{bmatrix} \tag{5}$$

The induced voltage generated by the sheath currents on the sheath can be calculated as follows:

$$\begin{bmatrix} \dot{E}_{\mathrm{s1}} \\ \dot{E}_{\mathrm{s2}} \\ \dot{E}_{\mathrm{s3}} \end{bmatrix} = \mathrm{j}\begin{bmatrix} 0 & X_{12}l_1 + X_{23}l_2 + X_{31}l_3 & X_{13}l_1 + X_{21}l_2 + X_{32}l_3 \\ X_{21}l_1 + X_{32}l_2 + X_{13}l_3 & 0 & X_{23}l_1 + X_{31}l_2 + X_{12}l_3 \\ X_{31}l_1 + X_{12}l_2 + X_{23}l_3 & X_{32}l_1 + X_{13}l_2 + X_{21}l_3 & 0 \end{bmatrix}\begin{bmatrix} \dot{I}_{\mathrm{s1}} \\ \dot{I}_{\mathrm{s2}} \\ \dot{I}_{\mathrm{s3}} \end{bmatrix} \tag{6}$$

where $\dot{I}_1$, $\dot{I}_2$, $\dot{I}_3$ are the core currents of phase A, B, and C, respectively, l_1, l_2, l_3 are the length of the three cross-interconnection segments, respectively, $\dot{E}_{t1}$, $\dot{E}_{t2}$, $\dot{E}_{t3}$ are the induced voltages of the sheath generated by the core currents, respectively, and $\dot{E}_{s1}$, $\dot{E}_{s2}$, $\dot{E}_{s3}$ are the induced voltages of the sheath generated by the sheath currents, respectively.

According to Kirchhoff's law,

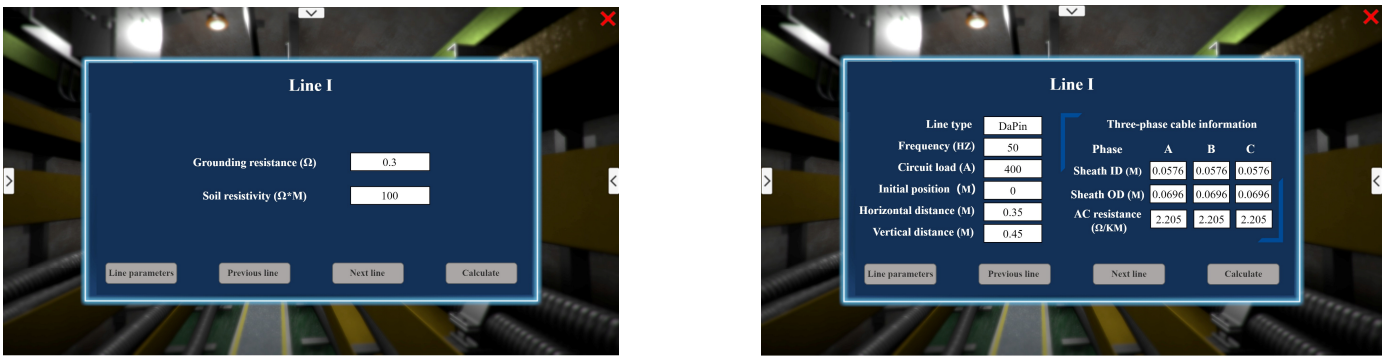
$$\begin{cases} Z_1\dot{I}_{\mathrm{s1}} + \left(R_{\mathrm{d1}} + R_{\mathrm{d2}}\right)\dot{I}_{\mathrm{se}} + \dot{E}_{\mathrm{s1}} = \dot{E}_{\mathrm{t1}} \\ Z_2\dot{I}_{\mathrm{s2}} + \left(R_{\mathrm{d1}} + R_{\mathrm{d2}}\right)\dot{I}_{\mathrm{se}} + \dot{E}_{\mathrm{s2}} = \dot{E}_{\mathrm{t2}} \\ Z_3\dot{I}_{\mathrm{s3}} + \left(R_{\mathrm{d1}} + R_{\mathrm{d2}}\right)\dot{I}_{\mathrm{se}} + \dot{E}_{\mathrm{s3}} = \dot{E}_{\mathrm{t3}} \\ \dot{I}_{\mathrm{se}} = \dot{I}_{\mathrm{s1}} + \dot{I}_{\mathrm{s2}} + \dot{I}_{\mathrm{s3}} \end{cases} \tag{7}$$

where $\dot{I}_{\mathrm{se}}$ represents the current in the cross-interconnection grounding point and the sheath current of a single-circuit cross-interconnection cable can be calculated according to Equations (1)–(7). The sheath currents of multi-circuit cables can be calculated by expanding the matrix of Equations (5)–(7).

3.2. Integration of the Simulation Model and the Tunnel Panoramic Digital Model

In this study, a 3D panoramic visualization system is developed and the tunnel panoramic digital model is displayed in the system. The sheath current simulation model proposed in this study is coded with MATLAB (Version R2023a). Subsequently, the more flexible and scalable Python language was selected to transcode the MATLAB source code and create data input/output interfaces, ensuring seamless communication with the 3D panoramic system. Given that the MATLAB simulation relies heavily on matrix operations, the NumPy library in Python was utilized to construct ndarray matrices and perform the corresponding computations. As the underlying simulation principles remain unchanged, the results obtained from the ported code are consistent with those of MATLAB, with computational performance comparable to MATLAB. Each single calculation is completed within a few seconds.

Figure 6 illustrates the integration of the simulation model and the panoramic digital model. The sheath current can be calculated online with the developed visualization system and the simulation results can be demonstrated via the 3D model, as shown in Figure 7. A dedicated data reading interface for the High-voltage Cable Lean Management Platform (HCLMP) was designed within the developed 3D panoramic system. The input parameters of the simulation model, such as the voltage level, circuit load, operating frequency, etc., of the cables, can be accessed directly from the HCLMP. Other input parameters of the simulation model, such as the spatial information of the cables (e.g., line spacing) and electrical information of the cables (e.g., sheath inner/outer diameter), are stored in the database of the developed system and can be invoked by the simulation model directly.



(**a**) (**b**)

Figure 6. Integration of the simulation model and online calculation. (**a**) Input parameters of the tunnel; (**b**) input parameters of cables.

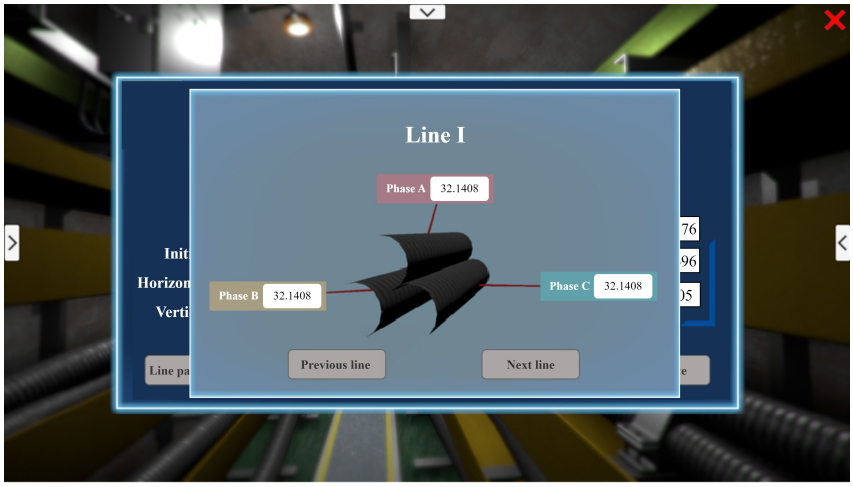


Figure 7. Simulation results demonstrated via the 3D model.

3.3. Validation of the Proposed Simulation Model

In this study, Line I and Line II laid in a tunnel in Beijing are modeled and used as a case study. Line I and Line II connect transformer stations A and B and run in parallel all along the tunnel, as shown in Figure 8. The layout of Line I and Line II is depicted in Figure 9. The three cables of Line I are arranged in an equilateral triangle formation, which is called "Xiao Pin Zi" in Chinese. The vertical distance and horizontal distance between these three cables are both 150 mm. The three cables of Line II are arranged in an isosceles triangle formation, which is called "Da Pin Zi" in Chinese. The vertical distance between the upper cable and the lower two cables is 450 mm, and the horizontal distance between the lower two cables is 350 mm. The vertical distance between the geometric centers of Line I and Line II is 800 mm. The cable model of both Line I and Line II is ZR-YJLW02-127/220KV-1 $\times$ 1000 mm^2. The distances between the three cross-connections are 467 m, 451 m, and 474 m, respectively.

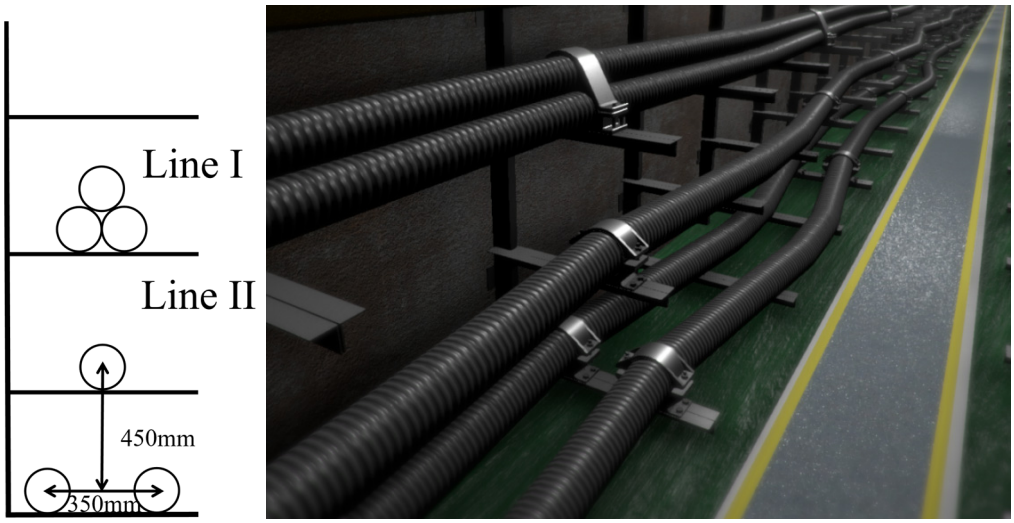


Figure 8. Schematic diagram of Line I and Line II laying in the tunnel.

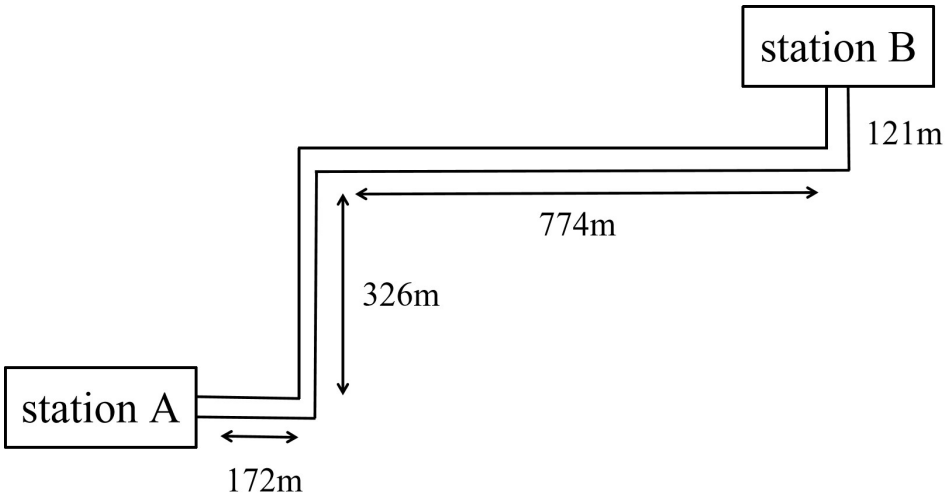


Figure 9. Graph of the layout of Line I and Line II.

During the core current analysis, when a certain moment is selected, the core currents of Line I and Line II are 332 A and 256 A, respectively. All the parameters used in the proposed simulation model are listed in Table 1.

Table 1. Parameters used in the proposed simulation model.

Parameter Name	Value	Parameter Name	Value
Core outer diameter/mm	48.5	Core cross-sectional/mm^2	1600
Conductor shield thickness/mm	2.0	Aluminum sheath resistivity/Ω·m	2.8264×10^{-8}
Insulation thickness/mm	24.0	Cable support spacing/mm	1680
Insulation shield thickness/mm	1.0	Height of each layer of bracket/mm	450
Thickness of metal sheath/mm	2.6	Spacing of cables in the form of large triangle/mm	350
Sheath thickness/mm	5.0	Ground resistance/Ω	0.3
Cable outer diameter/mm	135.2	Soil resistivity/Ω·m	300

The comparison between the monitored and calculated sheath current values is shown in Table 2. Since the cable has only one section of cross-linked connections, only the cable sheath current for a single cable segment needs to be calculated. Taking the monitored data from transformer station A as an example, as shown in Table 2, the calculated values are consistent with the measured values, with a maximum error of only 3.71%. The error is attributed to a few seconds' delay in the sensor data, meaning some sensors may not measure at the same time. Additionally, some cable segments were measured manually, which may result in discrepancies from the actual length. Overall, the proposed simulation model meets the accuracy requirements within the acceptable error range and accurately reflects the variations in sheath current.

Table 2. Comparison of monitored and calculated sheath current values.

Line Name	Phase Classification	Monitoring Value (A)	Calculated Value (A)	Inaccuracies (%)
I	Phase A	23.8	23.6	0.84
	Phase B	24.5	25.3	3.26
	Phase C	29.6	30.7	3.71
	Phase T	82.1	80.29	2.20
II	Phase A	28.8	29.5	2.43
	Phase B	25.4	25.9	1.96
	Phase C	23.7	23.3	1.68
	Phase T	77.2	78.4	1.55

4. Intelligent Decision Support for Cable Sheath Current Operation Based on the 3D Digital Model

4.1. Early Warnings Against Cable Sheath Current Anomalies

For the traditional sheath current monitoring and display system, the sheath current monitoring depends on the quality of the sensors and the stability of the communication system. If the corresponding point sensor or communication line is faulty, it is difficult to reflect the sheath current value in real time, and it is impossible to provide early warning information for the operation and maintenance management personnel.

For high-voltage cables, the current of the cable core is a key indicator of the power system. In this section, sheath currents at each point of Line I and Line II are calculated based on the simulation model proposed in this study. The sheath current differences between some common cable sheathing faults (e.g., sheath shorting, cross-interconnection box water ingress, sheath grounding, etc.) and normal conditions are analyzed. The fault location is presented intuitively on the 3D digital model of the tunnel, as shown in Figure 10.

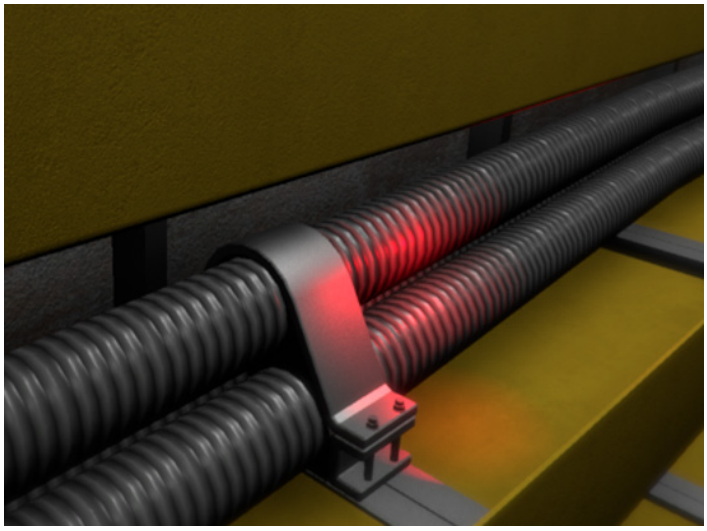


Figure 10. Real-time fault alert based on the 3D digital model.

ATP-EMTP software (Version 7.3) is used to establish the cable fault simulation model. Sheath currents under fault conditions are calculated based on the established fault model, and sheath currents under normal conditions are calculated based on the proposed simulation model in this study. Before performing fault detection, the system automatically analyzes the data timestamps from each sensor and decides whether to initiate a fault diagnosis based on the configured time threshold. To ensure the robustness of the detection system, if data from critical sensors are lost, the system will reject the fault detection request for that section of the line and notify the user to check the sensor status. Furthermore, the system currently includes response mechanisms for extreme fluctuations. When there is a rapid change in current, the system first records the current curve, then automatically triggers the defect and fault detection features. It will perform diagnostics of the line's operating status and issue corresponding early warnings. The comparison of the calculation results is shown in Table 3.

Table 3. Sheath current comparison under normal conditions and abnormal conditions.

Line	Phase Classification	Calculated Value (A)	Shorting of Two-Phase Sheaths (A)	Interconnection Box Misconnection (A)	Interconnection Grounding Box Water Ingress (A)
I	Phase A	23.6	298.3	167.5	328.0
	Phase B	25.3	26.8	207.1	335.8
	Phase C	30.7	308.2	207.8	332.3
	Phase T	80.29	77.7	72.8	71.4
II	Phase A	29.5	28.9	29.6	28.2
	Phase B	25.9	25.4	21.9	18.3
	Phase C	23.3	23.3	21.9	22.6
	Phase T	78.4	78.1	72.8	69.2

As shown in Table 3, after a wiring error occurs in the cable cross-interconnection system, the three-phase sheath-induced voltage is no longer symmetrical. There is a large difference between the faulty sheath current and the normal sheath current. By comparing the theoretically calculated values with the monitoring values, early warnings related to cable sheath currents can be realized.

4.2. Suggestions for Sheath Current Suppression Based on Phase Sequence Optimization

Reducing sheath current effectively lowers cable operating temperatures, minimizes power losses, enhances transmission efficiency, and slows insulation aging. This not only

extends the cable lifespan, but also reduces maintenance, replacement frequency, and cooling needs, significantly improving overall energy efficiency and lowering long-term operational costs. For laid high-voltage cables, the spatial location of the cable lines is fixed. The grounding impedance and the soil resistivity nearby have minimal impact on the cable circuits in the same tunnel. Consequently, if the sheath current needs to be suppressed and regulated, changing the arrangement of the phases or the spacing between phases is not feasible. The most effective option is to change the phase sequence of the core current. Compared to the traditional method of inserting series resistors, this method fundamentally controls the generation of sheath currents, avoiding overheating at resistor insertion points. It suppresses sheath current generation directly at the cable installation location.

Line I and Line II mentioned above are used as a case study in this section. For double-circuit cables on the same side of the tunnel, due to their axisymmetric characteristics and three-phase symmetry, there are only three possible phase sequence combinations, as shown in Table 4.

Table 4. Possible phase sequence arrangements of Line I and Line II.

Combination Number	Phase Sequence
1	ABC/ABC; ABC/CBA; CBA/ABC; CBA/CBA
2	ABC/ACB; ABC/BCA; CBA/ACB; CBA/BCA
3	ABC/BAC; ABC/CAB; CBA/BAC; CBA/CAB

Both Line I and Line II are arranged with the phase sequence of ABC. According to the monitoring records on the HCLMP, the core currents of Line I and Line II usually vary between 200 and 500 A. To calculate the optimal phase sequence, this study uses the historical load data of two circuits from the past year. By calculating the sheath current values under different phase sequence arrangements, different core currents under the sheath current are found, as shown in Figure 11.

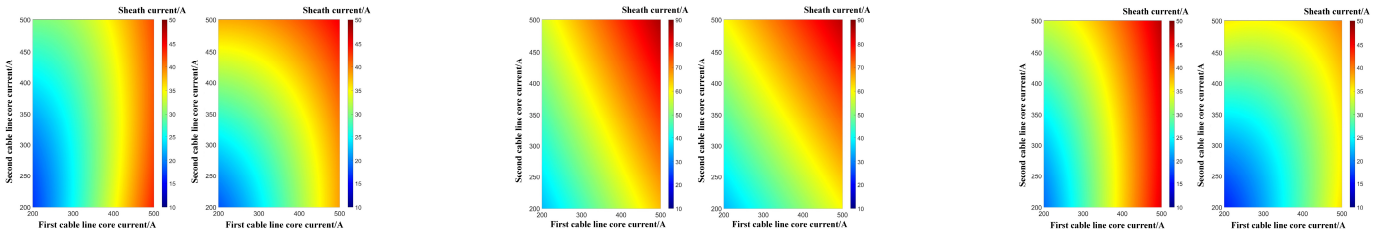


Figure 11. Calculated values of sheath current under different core currents for different phase sequence combinations. (**a**) Combination 1; (**b**) Combination 2; (**c**) Combination 3.

To analyze the impact of different phase sequences on the sheath current, this study takes Combination 1 as the baseline and compares the sheath current reduction ratios of phase sequence Combination 2 and Combination 3 with Combination 1. The comparison results are shown in Table 5.

Table 5. The reduction ratios of sheath current for different combinations.

Combination Number	Line I/%	Line II/%
a	0	0
b	51.8	43.7
c	45.2	48.2

As seen in Table 5, changing the cable phase sequence can effectively reduce the sheath current, thereby decreasing the probability of the grounding current exceeding the standard.

5. Discussion and Conclusions

5.1. Discussion

The proposed high-voltage cable sheath current simulation model, integrated with a 3D panoramic digital tunnel model, demonstrates considerable potential for improving the monitoring and management of power transmission networks. While the system has been successfully tested in controlled environments, such as Line I and Line II in Beijing, its deployment in large-scale urban power grids introduces additional complexities.

For large tunnels with high cable densities, the sheath current simulation algorithm reserves a data interface to support multi-circuit lines, theoretically enabling it to accommodate larger tunnels or networks with significantly higher cable densities. In fact, the algorithm has already been successfully implemented for the sheath current simulation of six-circuit lines in another tunnel in Beijing. The main challenge in deploying the 3D system in large-scale urban power grids lies in the 3D panoramic modeling and visualization. Large-scale urban tunnels, often extending several kilometers, result in substantial modeling workloads and pose significant challenges to visualization performance. Therefore, when deploying the 3D system in such environments, it may be necessary to reduce model accuracy in order to improve rendering efficiency. Alternatively, a 2D visualization system could be developed, integrating the proposed algorithm to mitigate the computational burden of 3D modeling.

Furthermore, the electrical structure of the cables (e.g., high-voltage cables are typically single-core, while low-voltage cables are multi-core) presents additional challenges in applying the proposed simulation. The simulation algorithm described in this study is currently limited to the sheath current simulation of high-voltage single-core cables with cross-linked metal sheath connections. When low-voltage multi-core cables are arranged in parallel within a tunnel, their electromagnetic induction effects could influence the sheath current simulation results. Future research may need to address the modeling and correction of electromagnetic interference from low-voltage multi-core cables, particularly in cases of inter-cable coupling.

Looking ahead, future developments will focus on integrating multi-physics fields with digital twin technology to enable the more accurate modeling of cable temperature gradients and mechanical stresses. This integration will enhance the predictive capabilities of the system, enabling the real-time monitoring of cable health and ultimately improving the safety, efficiency, and longevity of the power transmission infrastructure.

5.2. Conclusions

In this study, a three-dimensional panoramic digital model of a cable tunnel was modeled, a sheath current simulation model for parallel cables was proposed, and a visualization system was developed. The main conclusions of this study are as follows:

(1) A 3D digital panoramic model of a tunnel in Beijing was modeled using laser point cloud technology. A visualization system was developed, characterized by the intuitive display of the tunnel in a three-dimensional panorama, the online calculation of sheath current, the real-time inversion of sheath current at data-missing locations, and the optimization of cable phase sequences for abnormal sheath currents.

(2) A sheath current simulation model for parallel cables was proposed. Through case verification, the calculated sheath current results present a maximum measurement error of 3.71%. The cable fault recognition model was established with ATP-EMTP software. By comparing the calculated results with the monitored data, changes/fluctuations in the sheath current can be reflected. Integrated with the visualization system, an early warning can be triggered once the cable sheath current values are abnormal.

(3) For dual-circuit cables on the same side of a tunnel, the sheath current can be suppressed by altering the phase sequence of the core currents, with a maximum reduction in sheath current of up to 51.8%.

Author Contributions: Conceptualization, Z.P. and Y.L.; methodology, Z.P., W.G. and Y.M.; software, H.L., Y.L. and L.X.; validation, Z.P., Y.M. and S.X.; formal analysis, J.C. and L.X.; data curation, Z.P. and Y.L.; writing—original draft preparation, Z.P. and Y.W.; writing—review and editing, H.L.; supervision, Y.W.; project administration, Y.M.; funding acquisition, W.G. All authors have read and agreed to the published version of the manuscript.

Funding: This research was funded by the Science and Technology Project of STATE GRID BEIJING ELECTRIC POWER COMPANY (520223230015).

Data Availability Statement: The data presented in this study are available on request from the corresponding author due to confidentiality and legal restrictions regarding the data.

Conflicts of Interest: The authors declare no conflicts of interest.

References

1. Orton, H. Power Cable Technology Review. *High Volt. Eng.* **2015**, *41*, 1057–1067.
2. Yang, Y.; Hepburn, D.; Zhou, C.; Zhou, W.; Bao, Y. On-Line Monitoring of Relative Dielectric Losses in Cross-Bonded Cables Using Sheath Currents. *IEEE Trans. Dielectr. Electr. Insul.* **2017**, *24*, 2677–2685. [CrossRef]
3. Jung, C.; Lee, J.; Kang, J. Sheath Circulating Current Analysis of a Crossbonded Power Cable Systems. *J. Electr. Eng. Technol.* **2007**, *2*, 320–328. [CrossRef]
4. He, Y.; Meng, F.; Kok, L.; Ho, K. A K-to-Ka Band Ultra Wideband Power Amplifier in 180-Nm SiGe Technology. In Proceedings of the 2024 IEEE International Conference on IC Design and Technology, Singapore, 25–27 September 2024; pp. 1–4.
5. Liu, Y.; Xiao, Y.; Liu, S. Influence of Cluster Laying on Permitted Current Rating of Power Cables in Tunnels. *High Volt. Appar.* **2019**, *55*, 123–130.
6. Lu, P.; Duan, W.; Sun, J.; Zhao, X.; Xiong, L. Core Temperature Calculation of Single-Core Cable Joints Based on FEM. *Power Syst. Clean Energy* **2021**, *37*, 57–63.
7. He, X. Analysis of the Major Causes of Metal Sheath Grounding Loop Flow in High Voltage Single Core Cables. *Opt. Mech. Electr.* **2015**, *12*, 68–69.
8. Ma, F.; Niu, Z.; Luan, Y. Digital Supervision and Correlation Analysis of High-Voltage Cable Crimping. *Electr. Power Equip. Manag.* **2023**, *16*, 52–54.
9. Li, S.; Dong, Z. Research on Key Location Extraction Technology of Underground Cable Line Based on Digital Intelligent Terminal Platform. *Microcomput. Appl.* **2022**, *38*, 65–67.
10. Li, M.; Wu, Y.; Chen, G. Research and Application of Digital 3D Technology in Indoor Substation Cable Laying. *Electr. Eng.* **2023**, *9*, 88–90.
11. Yao, J.; Yang, Y.; Wang, X. Systematic review of digital twin technology and applications. *Vis. Comput. VCIBA* **2023**, *6*, 10. [CrossRef]
12. Qi, Q.; Tao, F.; Liu, A. Enabling technologies and tools for digital twin. *J. Manuf. Syst.* **2021**, *58*, 3–21. [CrossRef]
13. Guo, J.; Qi, D. Enhancement of damaged-image prediction based on digital twin technology. *J. Cloud Comput.* **2023**, *12*, 177. [CrossRef]
14. Yuan, B.; Ma, L.; Wu, Q. Cable Route and Channel Management System Based on 3D Laser Scanning Technology. *Rural Electrif.* **2023**, *10*, 41–43.
15. Zhong, S.; Fang, X.; Xu, H.; Xu, Z.; Fang, Y. Exploration on Digital Design of Electrical Cable Trays for Buildings. *Build. Electr.* **2023**, *42*, 46–51.
16. Bai, Y.; Guo, K.; Li, J.; Shi, H.; Hu, G. Automatic Statistical Method of Secondary Cable Length Based on Digital Three-dimensional Technology. *Ind. Appl. Commun.* **2024**, *43*, 173–177.
17. Li, X.; Song, P.; Meng, Z. Measurement Method for Reference Data of Power Cable Fiber Optic Temperature Measurement Based on Real-Life and Digital Model. Patent CN202311574923.3, 8 March 2024.
18. Zhang, Z.; Shu, N.; Zhao, J. Analysis and calculation the thermal stress and short circuit force of the power cable line. In Proceedings of the 2014 China International Conference on Electricity Distribution, Shenzhen, China, 23–26 September 2014; pp. 850–853.
19. Anders, G.; Brakelmann, H. Improving Cable Rating Calculation by Considering Loss Dependence on Temperature. *Trans. Power Deliv.* **2004**, *19*, 919–925. [CrossRef]
20. Nahman, J. Cable Models for Grounding System Analysis. *IEEE Trans. Power Deliv.* **2004**, *19*, 841–845. [CrossRef]
21. Wei, Y.; Liu, M.; Li, X. Effect of temperature on electric-thermal properties of semi-conductive shielding layer and insulation layer for high-voltage cable. *High Volt.* **2021**, *6*, 805–812. [CrossRef]
22. Zhang, Y.; Yu, F.; Ma, M. Conductor temperature monitoring of high-voltage cables based on electromagnetic-thermal coupling temperature analysis. *Energies* **2022**, *15*, 525. [CrossRef]
23. Zhou, W.; Li, W.; He, W.; Liang, J. Substation digitalized cable laying modeling and related calculation of cable carrier. *Mod. Electron. Tech.* **2022**, *45*, 166–172.

24. Zhu, L.; Wang, G.; Zhu, Y. Research on application of 3D design technology in cable laying of substation. *Mach. Des. Manuf. Eng.* **2021**, *50*, 121–126.
25. Zhu, G.; Qi, M.; Chen, X.; Wang, Z.; Yu, K. The Influence of Phase Spacing and Loop Spacing on Circulating Current of Power Cable Metal Sheath. *J. Northeast Electr. Power Univ.* **2021**, *41*, 79–85.
26. Wang, Y.; Cao, W.; Liang, H.; Li, F. Fitting Formula of Sheath Current and the Arrangement Optimization of Cables. *High Volt. Appar.* **2017**, *53*, 77–82.
27. Qi, M. Research on Circulation Characteristic and Suppression Measures of Metal Sheath of XLPE Cable. Master's Thesis, Northeast Electric Power University, Jilin, China, 2022.
28. Todorovski, M.; Ackovski, R. Equivalent Circuit of Single-Core Cable Lines Suitable for Grounding Systems Analysis Under Line-to-Ground Faults. *IEEE Trans. Power Deliv.* **2014**, *29*, 751–759. [CrossRef]
29. Shaban, M.; Salam, M.; Ang, S. Assessing Induced Sheath Voltage in Multi-Circuit Cables: Revising the methodology. In Proceedings of the 2015 IEEE Conference on Energy Conversion (CENCON), Johor Bahru, Malaysia, 19–20 October 2015.
30. Harun, Z.; Osman, M.; Ariffin, A. Effect of AC Interference on HV Underground Cables Buried Within Transmission Lines Right of Way. In Proceedings of the 2021 IEEE International Conference on the Properties and Applications of Dielectric Materials (ICPADM), Johor Bahru, Malaysia, 12–14 July 2021.
31. Chen, K.; Qi, W. Effect of Mixed Arrangement on Current in Sheaths of Two-circuit Arranged XLPE Cables. *High Volt. Eng.* **2018**, *44*, 3736–3742.
32. Jung, C.; Lee, J.; Kang, J. Sheath Current Characteristic and Its Reduction on Underground Power Cable System. In Proceedings of the IEEE Power Engineering Society General Meeting, San Francisco, CA, USA, 16 June 2005.
33. Fang, J.; Zhang, Y.; Liao, W. 110kV high voltage cable sheath transposition to reduce the grounding induction currents. *IOP Conf. Ser. Earth Environ. Sci.* **2022**, *983*, 162–167. [CrossRef]
34. Mao, X.; Kan, Y.; Zhang, Y. Analysis of Abnormal Ground Current in 110kV Cable Line. *IOP Conf. Ser. Earth Environ. Sci.* **2020**, *617*, 012030.
35. Jensen, F.; Nanayakkara, K.; Rajapakse, D. Online fault location on AC cables in underground transmission systems using sheath currents. *Electr. Power Syst. Res.* **2014**, *115*, 74–79. [CrossRef]
36. Yuan, Y.; Li, H.; Ren, Z.; Guo, W.; Lu, H.; Lan, L. Calculation of Zero-sequence Sheath Current and Load-phase Sequence Optimization Method for Double-circuit Parallel Laying High-voltage Cables. *Insul. Surge Arresters* **2022**, *3*, 123–132.
37. He, B.; Zhou, Y.; Li, H. Fault Identification of High-Voltage Cable Sheath Grounding System Based on Ground Current Analysis. In Proceedings of the 2020 IEEE 4th Conference on Energy Internet and Energy System Integration, Wuhan, China, 30 October –1 November 2020.
38. Yan, L.; Peng, F.; Chen, X. Study on Sheath Circulating Current of Cross-linked Power Cables. In Proceedings of the International Conference on High Voltage Engineering & Application, Chongqing, China, 9–12 November 2008.
39. *Q/GDW11316-2018*; Test Code for HV Power Cables. State Grid Corporation of China: Beijing, China, 2018.
40. *Q/CSG1206007-2017*; Regulations for Maintenance and Testing of Power Equipment. State Grid Corporation of China: Beijing, China, 2017.

Disclaimer/Publisher's Note: The statements, opinions and data contained in all publications are solely those of the individual author(s) and contributor(s) and not of MDPI and/or the editor(s). MDPI and/or the editor(s) disclaim responsibility for any injury to people or property resulting from any ideas, methods, instructions or products referred to in the content.